Available online at www.sciencedirect.com
SCIENCE DIRECT®
Respiratory Physiology & Neurobiology 148 (2005) 3–21
RESPIRATORY PHYSIOLOGY & NEUROBIOLOGY
www.elsevier.com/locate/resphysiol

Design of peripheral airways for efficient gas exchange

Ewald R. Weibel [a,*], Bernard Sapoval [b], Marcel Filoche [b]

[a] *Institute of Anatomy, University of Berne, Baltzerstarsse 2, CH-3000 Berne 9, Switzerland*
[b] *Laboratoire de Physique de la Matière Condensée, Ecole Polytechnique, Palaiseau, France*

Received 27 February 2005; received in revised form 25 March 2005; accepted 25 March 2005

Abstract

Peripheral airways combine branched tubes for ventilation with the gas exchanging alveoli in the pulmonary acini, defined as the complex of airways supplied by one first order respiratory or transitional bronchiole. In this part, the replenishment of oxygen at the alveolar surface occurs by a combination of convective air flow with diffusion of oxygen in the air. The transition between convection and diffusion depends on the morphometric properties of the airways. The design of the peripheral airways in the acinus of the human lung is described quantitatively on the basis of measurements obtained on casts of the acinar airways. Comparable data for rat and rabbit are also discussed. On the basis of this morphometric information, a typical path model for human acinar airways is derived. These studies also form the basis for advanced modeling studies of gas exchange and ventilation. In particular the problems occurring because of diffusional screening and the design conditions for minimizing this effect are discussed.

Keywords: Peripheral airways; Pulmonary acinus; Screening; Gas exchange; Diffusing capacity

1. Introduction

Gas exchange in the lung occurs over a very large surface of contact between air and blood that is established in lung parenchyma by the complex of alveoli and capillaries. This depends crucially on ventilation of this surface with fresh oxygen-rich air, or rather on an adequate replenishment of alveolar air with oxygen as it is absorbed by capillary blood that profusely flows over the surface to carry oxygen to the tissues. The rate at which oxygen is taken up depends on the rate of capillary blood flow, on the permeability of the air–blood barrier, and on the O_2 partial pressure difference between capillary blood and the alveolar air in the layer near the surface. Ventilation serves to maintain the O_2 head pressure high. The conditions for CO_2 discharge are basically the same, but of course in reversed order.

Ventilation of alveoli occurs in two steps: (1) upon inspiration oxygen-rich air flows into the lung driven by the pump action of respiratory muscles, in expiration O_2-depleted but CO_2-rich air is blown out; (2) in the depth of the lung, as we approach the peripheral airways, convection becomes weak and O_2 now diffuses towards the periphery, driven by the P_{O_2} gradient

* Corresponding author. Tel.: +41 31 302 0003; fax: +41 31 302 4503.
E-mail address: weibel@ana.unibe.ch (E.R. Weibel).

1569-9048/$ – see front matter © 2005 Elsevier B.V. All rights reserved.
doi:10.1016/j.resp.2005.03.005

that becomes established as O_2 is absorbed at the alveolar surface. For this to happen in an orderly fashion, a branched system of airways is constructed to connect all of the 300 million alveoli that constitute the gas exchanger to the trachea (Weibel, 1963, 1997a,b). A number of conditions must be fulfilled, such as that the many gas exchange units must be ventilated equitably, and that the work imposed by breathing should be minimal. This demands that the airway tree is designed in such a way as to optimize the physical conditions governing ventilation; to this end, different design strategies must come into play in the central and in the peripheral airways: favoring convection in the central and favoring diffusion in the peripheral airways. This is particularly critical in the peripheral airways where diffusion within the airways is combined with diffusive permeation of O_2 across the tissue barrier into the blood, the actual process of gas exchange.

In this system, the peripheral airways are something like the leaf-bearing twigs forming the vital ends of a branching tree: together with the alveoli and their associated capillaries they form the basic unit of the lung as gas exchanger, a unit called the acinus. Let us first consider the basic design of the airway tree, then the importance of design in the gas exchanger, in order to finally discuss how the two are joined to form a functional unit in the acinus.

2. Design of the airway tree

In the human and the mammalian lung the airways are built as dichotomous trees. This is the result of lung morphogenesis where the end bud of each airway tube gives rise to two daughter branches (Cardoso, 2000). In the human lung this goes on for 23 generations, on average, and since the number of branches doubles with each generation, there will be 2^{23} or about 8 million end branches, generally called alveolar sacs (Weibel, 1963). This is an average value; in reality the number of branching generations needed to reach the alveolar sacs is quite variable, ranging from about 18 to 30. This variability results from the fact that the airway tree forms a space-filling tree whose endings must be homogeneously distributed in space and reach into every corner and into every gap in the available space which is determined by the form of the chest cavity into which the lung develops. Some spaces are filled rapidly and the airways cannot continue to divide, whereas in other places more branches are needed to fill the space.

This branching process is accompanied by growth in length and diameter of the airway segments, the tubes between the branching nodes. The length of the tubes is adjusted to cover the distances needed to fill the space homogeneously with endings, whereas the diameter is, grossly speaking, made proportional to the size of peripheral lung that is supplied by this branch.

Fig. 1 shows portions of two casts of airway trees: (a) from a human lung and (b) from a rat lung. It is evident that in both instances airways branch by dichotomy and that the length and the diameter of the tubes become gradually reduced with each generation. There is, however, a marked difference in terms of the degree of irregularity of the branching pattern: in the human lung (Fig. 1a) the airway branching is to some extent symmetric, but in the rat lung there are large differences in the diameter and the length of the joint daughter branches and the branching pattern is quite asymmetric. This difference has largely to do with the shape of the space that must be filled: in the human lung that space is nearly "spherical" whereas in most quadrupedal animals the lung is longer and narrower. Accordingly, we find some main tracts of wider and longer airways to develop from which smaller airways branch off sideways to supply smaller units. This is less marked in the human lung (Fig. 1a) where the two branches of a parent bronchus often, though not always, show similar dimensions.

Despite a distinct degree of irregularity, some general rules govern the progression of dimensions along the tree (Weibel and Gomez, 1962; Horsfield et al., 1971). The diameter of daughter branches is smaller than that of the parent in the sense that the diameter reflects the volume of peripheral lung it supplies with air: larger airways serve larger lung units, smaller airways smaller units. The progression of airway diameters follows the law of Hess (1914) and Murray (1926) that the diameters of the daughter branches, d_1 and d_2, are related to the parent branch as $d_0^3 = d_1^3 + d_2^3$, or, for a symmetric tree $d_1 = d_2 = d_0 \cdot 2^{-1/3}$, a law that predicts optimization of the airway diameters for convective air flow, providing lowest resistance for lowest dead space volume (Weibel, 1963,1997a,b; Horsfield, 1997). A closer look at the airways of the human lung shows, however, that this is only approximately fulfilled as the lung appears to be designed with a certain safety factor

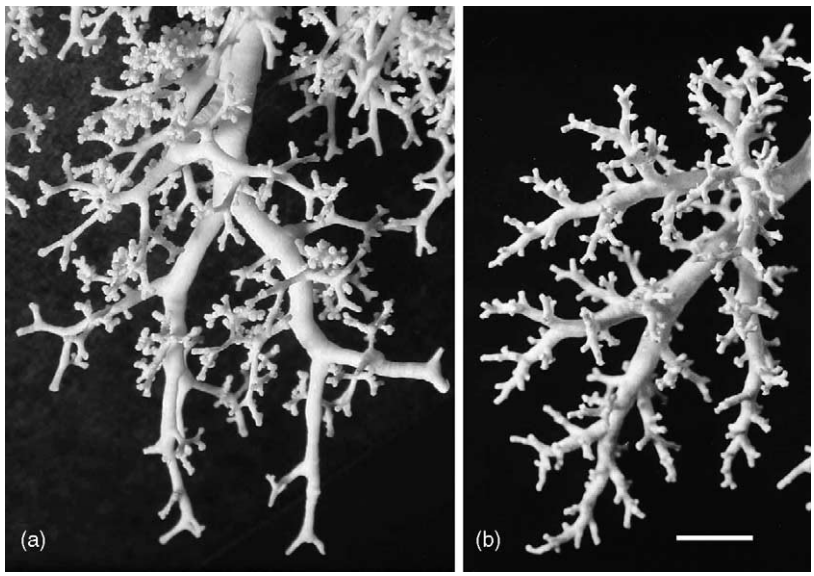

Fig. 1. Casts of peripheral conducting airways of (a) human lung, (b) rat lung. Scale marker 5 mm.

that allows regulation of air flow and avoids excessive resistance to flow (Mauroy et al., 2004).

These are the characteristics of the proximal airways built as smooth-walled tubes to distribute convective air flow into the lung. This design ends more or less abruptly when the airways reach lung parenchyma, the complex of alveoli that are arranged as a foam-like sleeve on the surface of peripheral airways (Fig. 2).

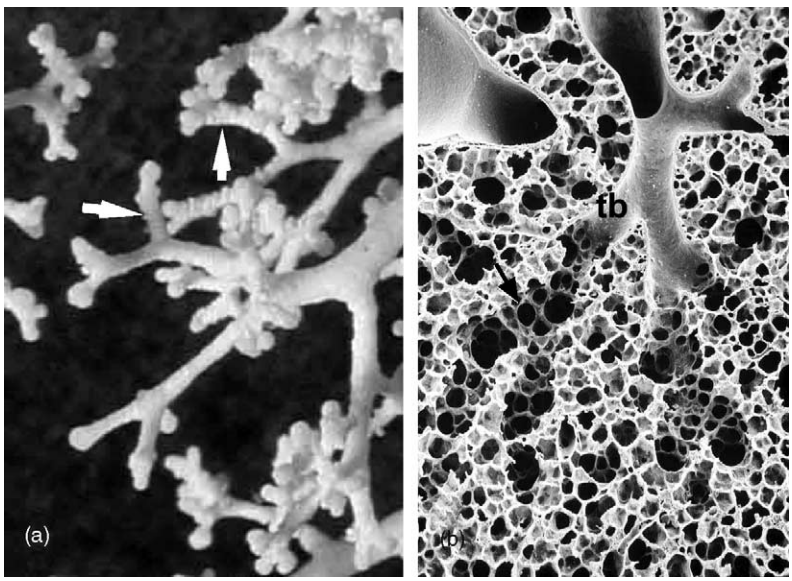

Fig. 2. Transition from conducting to acinar (respiratory) airways. (a) In cast of human lung (detail of Fig. 1a). (b) In scanning electron micrograph of perfusion-fixed rabbit lung the sequence of branched alveolar ducts following on transitional bronchiole (tb) is seen from inside. Note that alveoli appear on surface of respiratory bronchioles (arrows) in (a). In rabbit lung (b) the network of alveolar entrance rings that marks the (virtual) wall of the alveolar ducts is clearly seen (arrow).

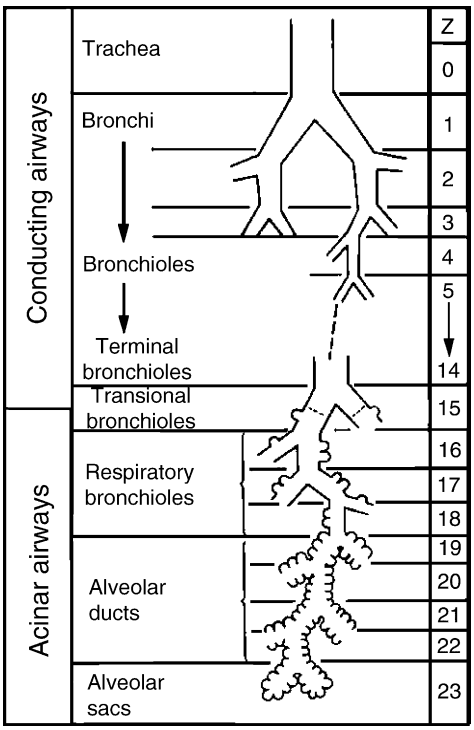

Fig. 3. Model of human airway system assigned to generations of symmetric branching from trachea (generation 0) to acinar airways (generations 15–23), ending in alveolar sacs. Modified after Weibel (1963).

Roughly speaking, this is the region of the airway tree where O_2 diffusion in the gas phase plays an important role in the supply of O_2 to the gas exchange surface. This is what we call the "peripheral airways", and it is justified to treat them as a special case because of the interaction of convection and diffusion in this part of the tree. The airway tree is thus subdivided into two major functional zones (Fig. 3): the first about 14–16 generations, on average, are designed as conducting airways where air flow is by convection; this is followed by about 8 generations of acinar airways where an axial channel, called alveolar duct, is enwrapped by a sleeve of alveoli with gas exchange tissue on their surface.

3. Design and fine structure of the gas exchanger

The pulmonary gas exchanger forms in the walls of the alveoli that contain a dense capillary network. Here, O_2 and CO_2 are exchanged between air and blood with great efficiency because of the intense contact between these two media over a very large surface and across a very thin tissue barrier (Weibel et al., 1991; Weibel, 1997b). The driving force for gas exchange is the partial pressure difference for O_2 between alveolar air and capillary blood, and this can only be maintained if the capillaries are perfused at a high rate, and the alveolar air is continuously replenished with O_2.

In order to allow efficient ventilation of the gas exchange surface, alveoli are arranged around the ducts, the continuations of the airway tree branching into lung parenchyma, and form a tightly packed sleeve of cup-like chambers that all open onto one duct (Fig. 4a). Adjacent alveoli are separated by septa that contain the capillary network. By this arrangement the alveo-

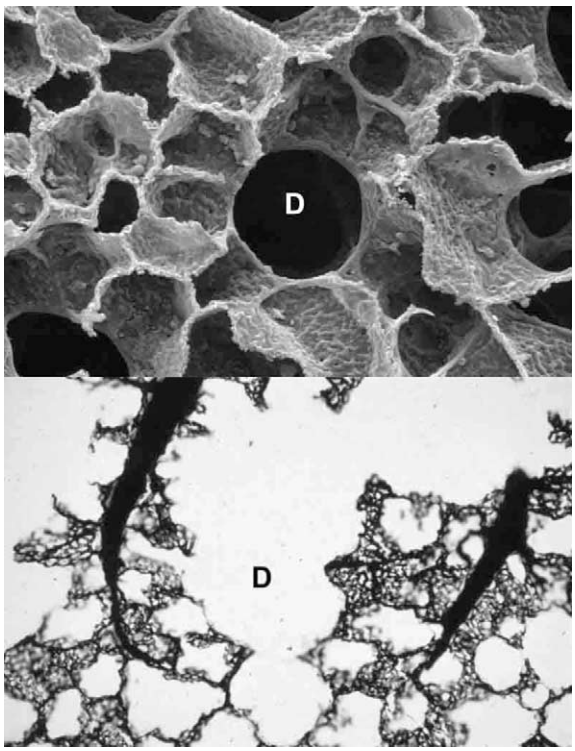

Fig. 4. (a) Scanning electron micrograph of cross-section of alveolar duct D in human lung showing densely packed alveoli surrounding the duct as the axial channel of the peripheral airways. (b) Equivalent region with alveolar duct D in rabbit lung where the capillary network contained in alveolar walls as well as the arteriole and a venule have been demonstrated with gold-labeling of blood plasma in a physiologically perfused preparation (König et al., 1993).

lar surface area available for gas exchange is about five times larger than the surface of the duct, but the diffusion distance for O_2 molecules from the duct to the gas exchanging surface remains small, on the order of 0.2 mm in the human lung.

The capillary network is also related to the conducting blood vessels. It appears as a continuum of flat networks within the connected inter-alveolar septa with which arterioles and venules are connected at multiple points (Fig. 4b) thus allowing the perfusing blood to spread broadly over the alveolar surface (König et al., 1993). It is noteworthy that the capillaries do not form networks that are associated with specific alveoli, even though the size of a capillary network unit – the region between an arteriolar and a venular ending – has about the same area as an alveolus. Capillaries are contained within the inter-alveolar septa and by that virtue exchange gases with two adjacent alveoli (Fig. 5). Furthermore, as alveolar septa form a three-dimensional maze after the pattern of soap bubbles or honey combs, the capillary network follows that geometry and also forms a three-dimensional complex of inter-connected flat network units (Fig. 5a).

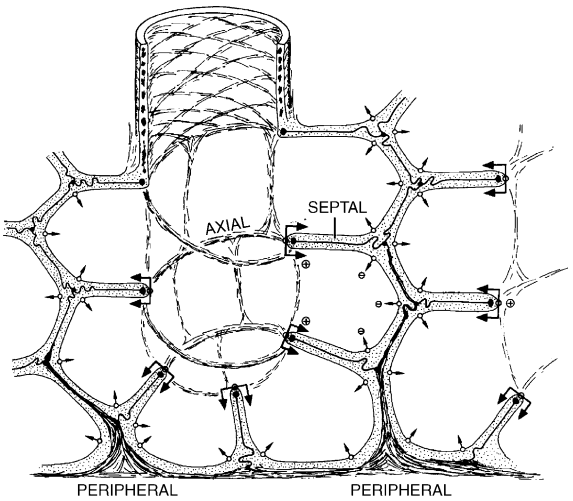

Fig. 6. Mechanical structure of basic acinar unit showing the alveolar septa supported by the pulmonary fiber continuum with septal fibers anchored on the peripheral and the axial fiber systems, the latter forming the "walls" of the acinar airways. From Weibel (1984).

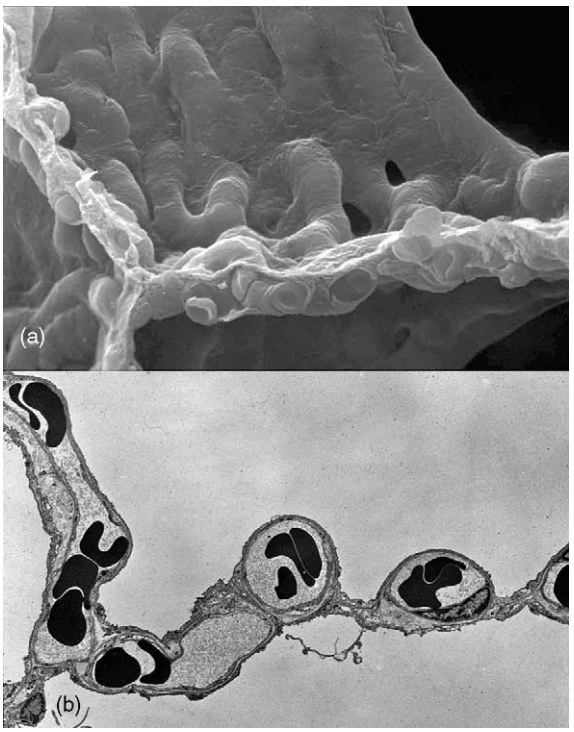

Fig. 5. Fine structure of the alveolar septum in human lungs shown in a scanning electron micrograph (a) and a thin section (b). Note thin tissue barrier separating the blood cells from the air.

The gas exchange tissue barrier that separates air and blood is very thin, on the order of 1 μm, but it is built of three tissue layers: alveolar epithelium and capillary endothelium separated by a thin interstitial layer (Fig. 5b). The cell layers ensure continued integrity whereas the interstitial connective tissue fiber system forms the support of the capillary network with which it is intertwined. It is part of a highly structured three-dimensional fiber continuum that extends from the pleura to the airway walls (Fig. 6). The respiratory movements are thus directly transmitted to the alveolar septa that thus remain well expanded in the parenchymal airspace (Weibel and Bachofen, 1987a,b, 1997). In the acinar peripheral airways the septal fibers are suspended between interlobular connective tissue septa and the fiber rings around alveoli that form the actual "wall" of the acinar ducts (Figs. 4a and 6). This tight association of the capillary network with the parenchymal fiber system, together with the surface-active alveolar lining layer, ensures that the gas exchange surface is maintained expanded and the air–blood barrier remains thin (Gil et al., 1979; Bachofen et al., 1983; Wilson and Bachofen, 1982).

These design properties affect the gas exchange conditions by setting the pulmonary diffusing capacity for oxygen, $D_{L_{O_2}}$, which determines oxygen uptake rate, $\dot{V}_{O_2}$, together with the O_2 partial pressure difference between air and blood as driving force, according to (see Weibel, 1997a):

$$\dot{V}_{O_2} = (P_{A_{O_2}} - P_{b_{O_2}}) D_{L_{O_2}} \quad (1)$$

Here, $P_{A_{O_2}}$ is the O_2 partial pressure in the layer of air adjacent to the gas exchange barrier, which is affected (1) by the extraction of O_2 by the blood and (2) by the rate at which O_2 is replenished by alveolar ventilation; the conditions for this will be a major issue in the following. The mean O_2 partial pressure of capillary blood, $P_{b_{O_2}}$, is determined (1) by the mixed venous P_{O_2} of the blood flowing in through the pulmonary arteries, (2) by the rate of capillary perfusion and transit time, (3) by the hemoglobin or erythrocyte content of capillary blood, and (4) by the rate of O_2 uptake from the air.

The pulmonary diffusing capacity, $D_{L_{O_2}}$, is largely determined by the design properties of the gas exchanger, mainly the alveolar and capillary gas exchange areas, S(A) and S(c), the capillary blood volume, V(c), and the harmonic mean thickness of the air–blood barrier, τ_{hb}. The model for calculating $D_{L_{O_2}}$ from these morphometric parameters splits the diffusion path into a membrane and a blood conductance, D_M and D_b, respectively, whose reciprocal values (the resistances) are summed to obtain the total resistance:

$$D_L^{-1} = D_M^{-1} + D_b^{-1} \quad (2)$$

$$D_M = K_{O_2} \frac{S(A) + S(c)}{\tau_{hb}} \quad (3)$$

$$D_b = \theta_{O_2} V(c) \quad (4)$$

The permeability of the membrane or barrier is determined by the Krogh permeability coefficient K_{O_2} for tissue, which is estimated at 3.3×10^{-8} cm^2 min^{-1} mmHg^{-1} (see Weibel et al., 1993). D_b is essentially determined by the binding rate of capillary blood for oxygen through the parameter θ_{O_2}, which in turn is affected by the red cell concentration or the hematocrit of capillary blood. This model and its application is extensively discussed in Weibel (1989,1997a).

Table 1
Morphometric estimate of human diffusing capacity[a]

Body mass (kg)	74 ± 4
Alveolar surface (m^2)	130 ± 12
Capillary surface (m^2)	115 ± 12
Capillary volume (ml)	194 ± 30
Tissue barrier thickness (μm)	0.62 ± 0.04
Total barrier thickness (μm)	1.15 ± 0.01
Diffusing capacity	
$D_{L_{O_2}}$	158 ml O_2 min^{-1} mmHg^{-1}
$D_{M_{O_2}}$	350 ml O_2 min^{-1} mmHg^{-1}
O_2 consumption	
$\dot{V}_{O_2}$ max	3700 ml O_2 min^{-1}

[a] Data from Gehr et al. (1978) and Weibel et al. (1993).

Table 1 shows the data obtained on normal human lungs (Gehr et al., 1978) from which we can estimate the pulmonary diffusing capacity. We find the gas exchange surface to be on the order of 130 m^2, the capillary volume about 200 ml, and the barrier thickness 1.1 μm resulting in an estimated diffusing capacity of 158 ml O_2 min^{-1} mmHg^{-1}. This means that for a P_{O_2} difference of 1 mmHg the pulmonary gas exchanger can transfer 158 ml O_2 from the air to the hemoglobin in erythrocytes; to achieve an O_2 uptake of 4 l min^{-1} as required by a human running at $\dot{V}_{O_2}$ max a P_{O_2} difference of 30 mmHg is needed. Since D_L is the "capacity" of the lung for diffusive uptake of O_2, we would predict that it is proportional to maximal rate of O_2 consumption $\dot{V}_{O_2}$ max. This prediction is only partly supported by the experimental test. We first find that the physiological diffusing capacity of a normal human is estimated at 30 at rest and at about 100 ml O_2 min^{-1} mmHg^{-1} in heavy exercise so that it appears the lung is designed with an excess diffusing capacity of about 30%; this can be interpreted as a "safety factor" in several respects: (1) athletes can increase their oxygen consumption by about 30% but evidence shows that the lung cannot adjust the size of its gas exchange structures to the same degree; (2) the alveolar P_{O_2} as the driving force for oxygen uptake is affected by the P_{O_2} in ambient air which can be variable, e.g. reduced at high altitude. Alveolar P_{O_2} can, of course, also be reduced if alveolar ventilation is inadequate.

This is also of interest in the context of comparative physiology, in particular with respect to the effects of variations in body size and exercise capacity of mammals (Weibel and Taylor, 1981; Weibel et al., 1987).

Studying athletic and non-athletic species we find that $D_{L_{O_2}}$ is not proportional to $\dot{V}_{O_2}$ max; comparing dogs and goats, for example, we find that $D_{L_{O_2}}$ is only 1.8 times greater in dogs than in goats as compared to a factor of 2.5 for $\dot{V}_{O_2}$ max (Weibel et al., 1987). It turns out that the dog's diffusing capacity is just what this athletic animal needs whereas the goat has an excess diffusing capacity, similar to the normal human (Karas et al., 1987). If we then look at allometric variation, we see that $D_{L_{O_2}}$ and $\dot{V}_{O_2}$ max have different slopes: $D_{L_{O_2}}$ increases about linearly with body mass whereas $\dot{V}_{O_2}$ max varies with the 0.86 power of body mass (Weibel et al., 1991). As a result, a 30 g animal, like a mouse, has a diffusing capacity per unit body mass that is about three times that of a cow of 500 kg, but it must accommodate an O_2 flow rate, which is eight times greater. In our context, this is an interesting observation because it tells us that a larger lung seems to have a larger excess $D_{L_{O_2}}$ compared with smaller animals. Could this perhaps be an adaptation to differences in the driving force for O_2 diffusion, in particular: could the alveolar P_{O_2} be lower in large species than small ones? This could be related to size differences in the acinar airways, as we shall further discuss below.

4. The acinar airway system connected to the gas exchanger

By all definitions the pulmonary acinus is the terminal unit of the respiratory airways that are directly associated with the gas exchanging surface. To define it as a consistent unit of the gas exchanger, we must decide on where along the airway tree the transition to the acinus occurs. The most precise definition is that the pulmonary acinus comprises the branched complex of alveolated airways that are connected to the same first order respiratory or transitional bronchiole. Since the acinus is a tree-like structure, this definition would identify the transitional bronchiole as the stem of the acinus (Rodriguez et al., 1987; Haefeli-Bleuer and Weibel, 1988).

The use of the traditional "terminal bronchiole" as the stem of the acinus must be abandoned because some transitional bronchioles branch off *before* the bronchiole ends (Fig. 7). This is particularly pronounced in animal lungs that, in general, show a greater degree of asymmetry than the human lung (Fig. 1). This is shown

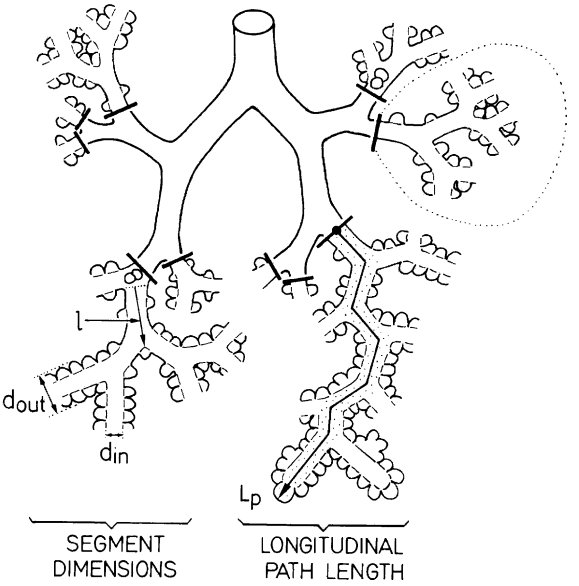

Fig. 7. Acini are defined as originating at transitional bronchiole (marked by a cross bar) where the first alveoli appear. The dimensions of the airway segments and of the longitudinal path length are defined. From Haefeli-Bleuer and Weibel (1988).

graphically in Fig. 8 on one segment of the right upper lobe of the rat lung shown in Fig. 1b. As a result of this asymmetric branching and asymmetric termination of the conducting airway tree the origin of acini is located in a broad range of generations of airway branching. The two graphs at the bottom of Fig. 8 show the frequency distribution of transitional bronchioles with respect to total airway generations. In the rat these generations range from 8 to 25 with a mean of 15 whereas in the rabbit the range is from 12 to 26 with a mean of 19 (Rodriguez et al., 1987). In the human lung, Schreider and Raabe (1981) showed that the spread is smaller because the airway tree is less asymmetric in its branching pattern (Fig. 1). From the measurement of mean acinar volume, we have estimated that there must be about 30,000 acini in an adult human lung, which on a dichotomous tree would locate them at generation 14–15. The range of variation is more difficult to estimate in the human lung, but from the distribution pattern of airway diameters it would appear that the standard deviation of generation number is on the order or ±3–4 generations.

In order to study the geometry and morphometry of pulmonary acini, one can fill the airways in a controlled

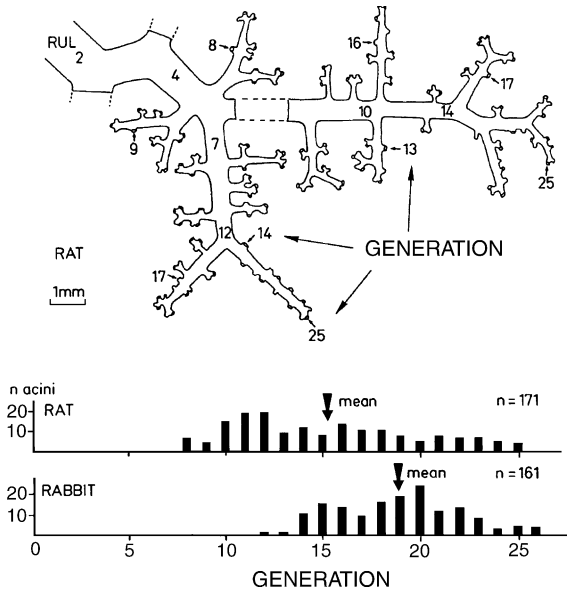

Fig. 8. Distribution of transitional bronchioles along one branch of the right upper lobe in rat and rabbit (compare Fig. 1b). From Rodriguez et al. (1987).

fashion with low viscosity silicone rubber, which can reach out to the very periphery of the air space system (Schreider and Raabe, 1981). After polymerisation, the tissue is removed by digestion and a preparation such as that shown in Fig. 9 results. The tissue septa have left fine clefts which can now be followed to dissect the airways along the conducting airway tree (Fig. 1), all the way out to peripheral branches where the occurrence of the first alveolar pockets indicate the presence of a transitional bronchiole, i.e. the initial branch of an acinus. This dissection is, by the way, helped by the fact that the pulmonary arteries that closely follow the airway tree are also dissolved away so that they leave a channel along which to dissect all the way into the acinus (Fig. 9a). The size of a human pulmonary acinus is on the order of a few millimetres in diameter. Microscopic dissection then allows the different internal tracts to be separated (Fig. 9b) and the airway system measured (Schreider and Raabe, 1981; Rodriguez et al., 1987; Haefeli-Bleuer and Weibel, 1988).

In a systematic study of three human lungs prepared by this method (Haefeli-Bleuer and Weibel, 1988) the mean volume of acini was found to be 187 mm^3 with a standard deviation of 79 mm^3. In small rodents the acini are very much smaller with a mean volume of 1.9 mm^3 in the rat and 3.46 mm^3 in the rabbit (Rodriguez et al., 1987). We will see, however, that the human acinus is not strictly comparable to that of rat and rabbit because at least three generations of acinar airways, the respiratory bronchioles, have only very few alveoli in their wall and thus contribute little to gas exchange (Fig. 9b). The comparable unit is something like the 1/8 acinus whose averaged volume is then about 23 mm^3.

It is noteworthy that the diameter of the transitional bronchiole, the stem of the acinus, is weakly, but significantly, related to the air volume it supplies, at least within each species. The diameter of an average transitional bronchiole measures 0.49 mm in the human lung. For the very much smaller acini of rat and rabbit lungs,

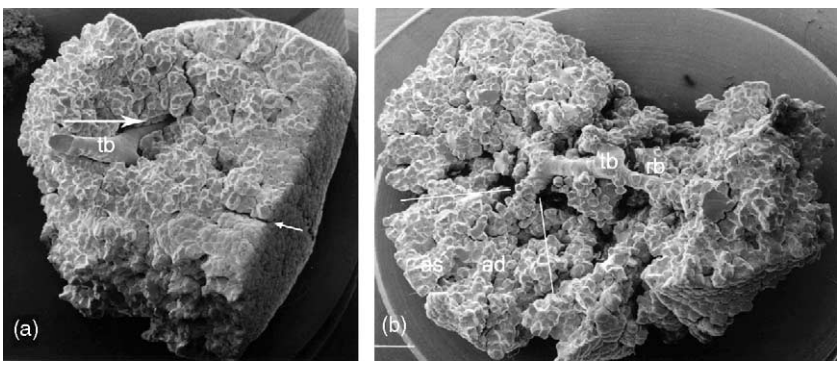

Fig. 9. (a) Scanning electron micrograph of a complete acinus from a silicon rubber cast of a human lung. Note transitional bronchiole (tb) with a few alveoli. Large arrow marks the channel left by the pulmonary artery branch that feeds into this acinus, the small arrow one of the pleural septa (peripheral fiber system, Fig. 6). (b) Partly dissected acinus from human lung showing transitional (tb) and respiratory (rb) bronchioles as well as alveolar ducts (ad) and alveolar sacs (as). Lines mark approximate boundary of 1/8 subacinus. From Haefeli-Bleuer and Weibel (1988).

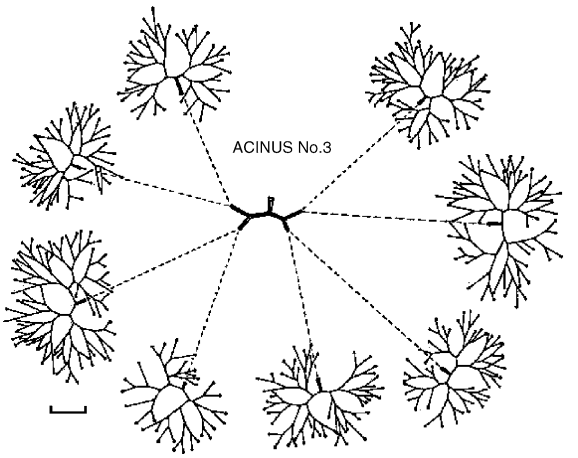

Fig. 10. Graphic representation of branching pattern of acinar airways in one human acinus of 183 mm^3 volume with the segment lengths drawn to scale. The airways are separated at the third generation thus displaying the branching pattern within each 1/8 subacinus. Scale bar 2 mm. From Haefeli-Bleuer and Weibel (1988).

this diameter is about 0.24 mm. The branching pattern for an average size human acinus is shown in Fig. 10. The segment lengths have been drawn to scale and the terminal clusters of alveoli of the alveolar sacs are marked by a dot. This acinus has been subdivided into its eight subacini whose subsystems are located in the third generation of acinar airways. The acinus shown in Fig. 9b is comparable in size and structure. The transitional bronchiole and the two subsequent generations of respiratory bronchioles are clearly visible. By dissecting off part of the acinar cast a 1/8 subacinus is exposed. Fig. 10 shows that the intra-acinar airways branch by irregular dichotomy; the number of segments doubles out to six generations and then begins to drop off as the terminal sacs are reached (Fig. 11). It can be seen that terminal sacs are located in generations 6–11 so that the intra-acinar airways branch over an average of 8–9 generations. There is some variation in this branching pattern, but on the whole the branching pattern of intra-acinar airways in rat and rabbit lungs is very similar with terminal generations located in generations 5–10, with an average generation number of 6–7 (Fig. 12). This indeed signifies that the high degree of asymmetry noted for the conducting airways of the rabbit lung (Fig. 1b) is no longer prevalent in the acinar airways where branching is much more symmetric.

The morphometry of the intra-acinar airways of the human lung shows a number of characteristic traits

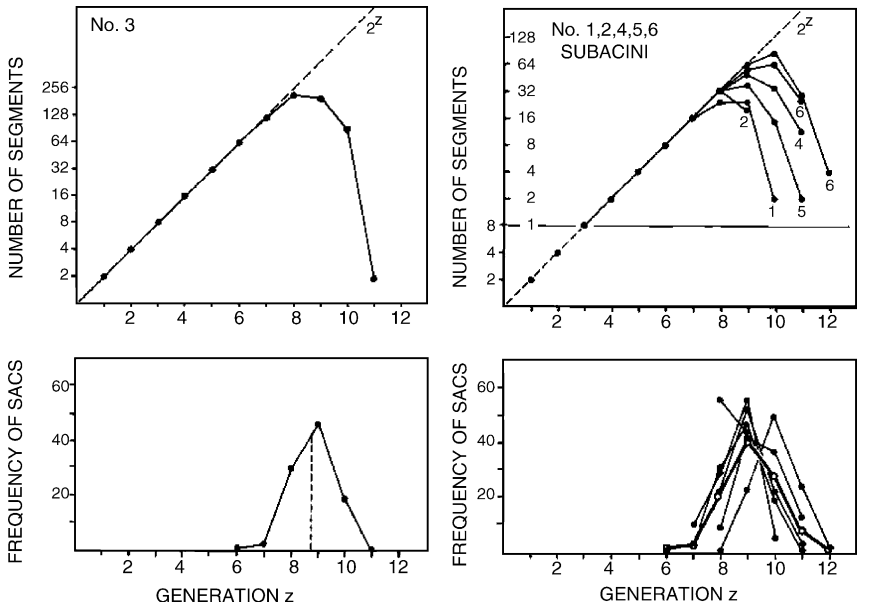

Fig. 11. The upper two graphs show the number of segments in each generation which increases by factor of 2 until the branching ends with the appearance of alveolar sacs. The lower graphs show the frequency distribution of alveolar sacs per acinar generation for human acini. The graphs on the left refer to the acinus shown in Fig. 10, those on the right to five other acini with the overall frequency distribution for all acini (heavy line and open dots). From Haefeli-Bleuer and Weibel (1988).

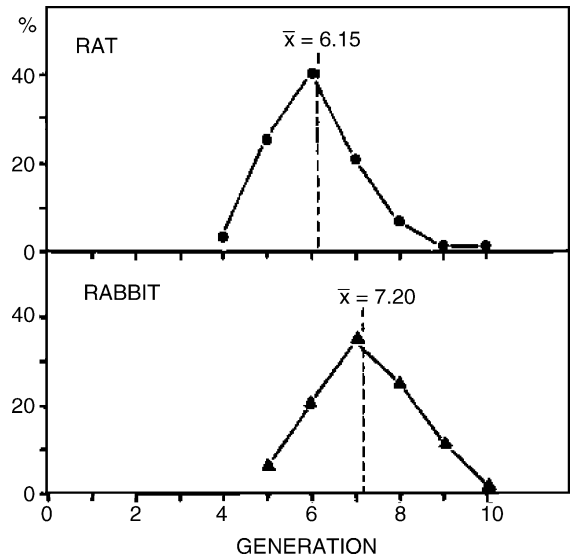

Fig. 12. Frequency distribution of alveolar sacs with respect to acinar generation for rat and rabbit. From Rodriguez et al. (1987).

(Haefeli-Bleuer and Weibel, 1988). Fig. 13 shows the average values for the length and diameter of the intra-acinar airways. The length of alveolar ducts gradually decreases from 1330 μm in generation 1 to 640 μm in generation 10. It is interesting that the length of the

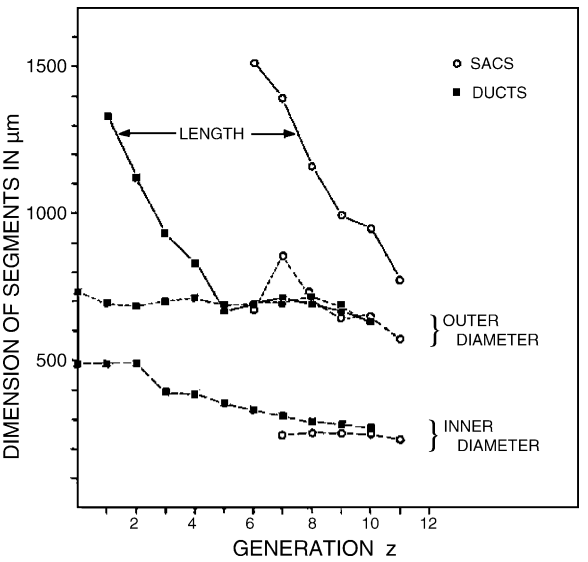

Fig. 13. Variation of length and diameter of acinar airways with progressive generation of branching, mean values for all human acini. From Haefeli-Bleuer and Weibel (1988).

alveolar sacs is greater than that of ducts located in the same generation. The reason is that the duct length comprises the depth of the terminal cluster of alveoli, which amounts to about 250 μm. Two characteristic values are estimated for the diameter of intraacinar airways: the inner diameter d_{in}, which characterizes the cross-section of the duct tube, and the outer diameter d_{out}, which comprises the entire sleeve of alveoli enwrapping the duct (see Fig. 7). The inner diameter of human acinar airways decreases from about 500 μm at the transitional bronchiole to 270 μm in generation 10; the inner diameter of alveolar sacs is about 250 μm for all generations. It is noteworthy that the outer diameter is nearly constant at 700 μm for all intra-acinar airways. The difference between outer and inner diameter reflects the mean depth of the alveolar sleeve, which therefore increases somewhat towards the periphery.

An important morphometric characteristic of acinar airways is the total path length for O_2 diffusion from the entrance at the transitional bronchiole to the terminal cluster of alveoli at the alveolar sac (Fig. 7). This path length is determined by two factors: the number of generations and the segment length. Accordingly, we can expect this path length to vary considerably. Fig. 14 shows that the average longitudinal path length amounts to 8.3 mm with a standard deviation of 1.4 mm. Considering the geometry of the acinus (Fig. 10), we note that of this total path length 3.4 mm are for the first three generations of respiratory bronchioles whereas the path length of alveolar ducts and sacs comprised in the 1/8 subacinus (Fig. 10) averages 4.7 ± 0.88 mm. In the much smaller acini of rat and rabbit the mean longitudinal path length is 1.46 ± 0.32 mm for the rat and 1.95 ± 0.36 mm for the rabbit. A small correction is necessary in view of discussing these path lengths with respect to functional processes. First, we must note that the transitional bronchiole is clipped off and therefore only partially contained in the cast (Figs. 7 and 9b) so that about 0.5 mm must be added to the path length. On the other hand, we must subtract 0.25 mm for the depth of the terminal cluster of alveoli at the end of the pathway.

With these data in hand, we can now first attempt to put the acinar airway dimensions into the perspective of the human airway tree, and then define an idealized model acinus. We first estimated that the human lung should contain some 26,000–32,000 acini (Haefeli-Bleuer and Weibel, 1988). With dichotomous

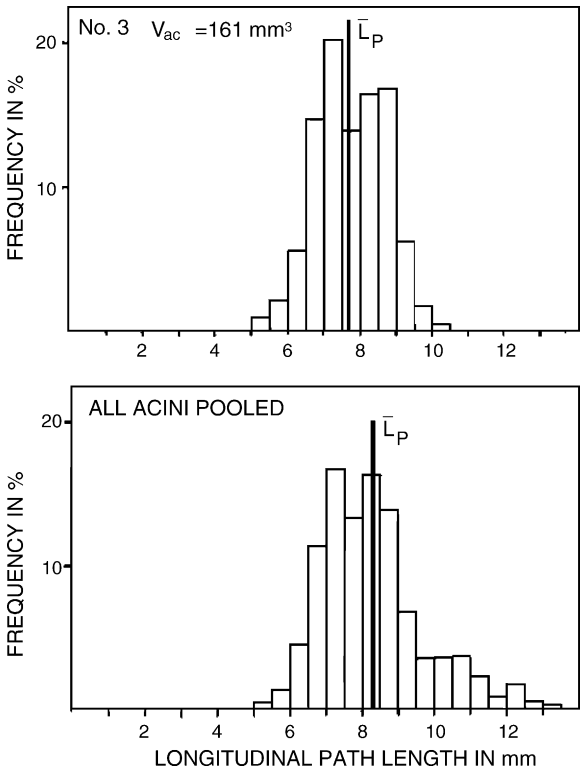

Fig. 14. Frequency distribution of longitudinal path length in human acini. From Haefeli-Bleuer and Weibel (1988).

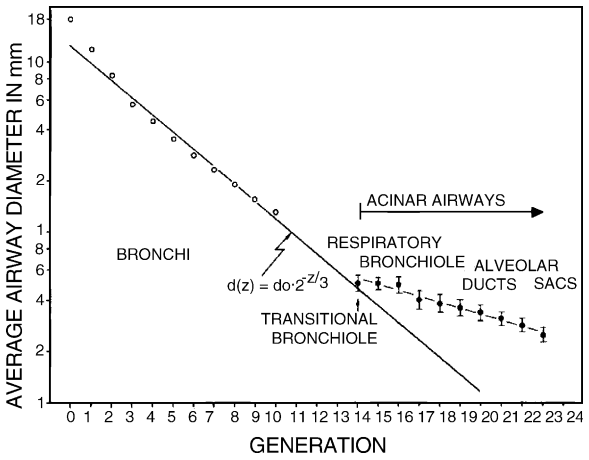

Fig. 15. In a symmetric model of human airways the acinar airway diameter is reduced less steeply with progressive generations than the conducting airways. From Haefeli-Bleuer and Weibel (1988).

branching, this would locate the airway entrance of the acini, the transitional bronchiole, at generations 14–15. The average number of 8–9 intra-acinar branching generations would bring the terminal alveolar sacs into generations 23–24, the number of total generations originally estimated for the human lung (Weibel and Gomez, 1962; Weibel, 1963). The average inner diameters of these airways can now be plotted onto the graph relating the average airway diameter to generation number in the human lung (Fig. 15). It can be seen that the average diameter of the transitional bronchiole falls onto the theoretical regression line predicted by the Hess–Murray law (Hess, 1914; Murray, 1926) and plotted through the estimated mean diameters of the bronchial tree. It is evident that the inner diameter of acinar airways does not decrease with the same slope as that for conducting airways as the diameter reduction from the transitional bronchiole to the terminal sac over nine generations is only by a factor of 1/2. This confirms the original observation that the diameter of intra-acinar airways fall less steeply than that of conducting airways and is thus larger than the prediction from the cube root of 1/2 rule (Hess–Murray law).

5. Typical path model of human acinus

We should now attempt to synthesize the wealth of data obtained on the acini of human lungs and to develop what we may call a typical path model for an average human acinus. Such an acinus has a volume of 0.187 cm^3. Its airways branch over eight generations in order to reach the terminal alveolar sacs (Fig. 11); in a first stage we will disregard the variation in this branch number and take the mean as the typical pattern. (The irregular branching number is necessary in order to homogeneously and completely fill the space available, but this aspect is now of secondary importance.) Table 2 shows that, in this idealized model, the branch number per generation z' increases as $2^{z'}$. Locating the transitional bronchiole ($z' = 0$) in generation 15 (Fig. 3) the terminal air sacs are in generation 23 of the typical path airway tree. The lengths and inner diameter of the airway segments are derived from Fig. 13 whereby the length of the alveolar sacs was reduced by 0.25 mm for the depth of the terminal alveolar cluster. The dimensions here given therefore characterize the

Table 2
Idealized typical path model of acinar airways: regularized dichotomy between transitional bronchiole (generation 0) and terminal alveolar sacs (generation 8)

Generation	Segments			Dimensions per generation				Path length[b]
z'	$N(z')$	l (mm)	d_{in} (mm)	$A_d(z')$ (mm^2)	$V_d(z')$ (mm^3)	$S_d(z')$ (mm^2)	$S_{alv}(z')$[a] (mm^2)	$L_p(z')$ (mm)
0	1	1.4	0.50	0.20	0.32	2.52 (0.2)[a]	7	1.4
1	2	1.33	0.50	0.39	0.52	4.18 (0.4)[a]	23	2.73
2	4	1.12	0.49	0.75	0.84	6.90 (0.7)[a]	67	3.85
3	8	0.93	0.40	1.00	0.93	9.35	129	4.78
4	16	0.83	0.38	1.81	1.50	15.85	219	5.61
5	32	0.70	0.36	3.26	2.28	25.3	349	6.31
6	64	0.70	0.34	5.81	4.07	47.9	661	7.01
7	128	0.70	0.31	9.11	6.38	87.3	1204	7.71
8	256	0.70	0.29	16.9	13.47	197.1	2720	8.41

Modified after Haefeli-Bleuer and Weibel (1988); $N(z')$: number of branches per generation; l: mean length; d_{in}: mean inner diameter of segments; $A_d(z')$: total cross-sectional area; $V_d(z')$: total air duct volume; $S_d(z')$: total duct surface; $S_{alv}(z')$: total alveolar surface per.

[a] Total alveolar surface of average acinus of 54 cm^2 is divided to the generations in proportion to the duct surface $S_d(z')$, reduced by the fraction (in parenthesis) of surface that is alveolated in respiratory bronchioles (generations 0–3), generation 8 including terminal cluster of alveoli.

[b] From entrance of transitional bronchiole to end of generation z'.

duct pathway and disregard, in a first step, the alveolar spaces that enwrap the ducts and sacs—note, however, that for these acinar airways the tube wall is virtual and is simply marked by the network of alveolar entrance rings (Figs. 2 and 4) that are the axial part of the supporting fiber system (Fig. 6). Table 2 reports the total airway cross-section per generation, $A_d(z')$, which is a determinant of air flow velocity, as well as the total duct volume and surface area, $V_d(z')$ and $S_d(z')$, respectively. These are calculated for simple cylindrical tube models of diameter d_{in} and length l without correction for the overlaps at the branch points. On the other hand, the alveolar sacs were considered to end with a hemispheric surface of diameter d_{in} around which the terminal cluster of alveoli is arranged (Fig. 7). Finally, the alveolar surface area was distributed to the different generations in proportion to the duct surface $S_d(z')$, but adjusting for the fact that only part of this surface is associated with alveoli in the respiratory bronchioles (generations 0–2). For an estimated alveolar surface of 130 m^2 in the human lung (Gehr et al., 1978) there would be about 54 cm^2 per average acinus of 0.187 cm^3 (this surface is lower than that assumed by Haefeli-Bleuer and Weibel, 1988, which had been an overestimate). It is seen that about half this gas exchange surface is in the last generation. A final check of this model is that the path length from the entrance into the transitional bronchiole to the end of the alveolar sacs is 8.4 mm, which agrees well with the mean path length estimated in the human acini (Fig. 14).

On the basis of Fig. 14 one could also begin to construct more realistic model acini that account for the variability in the number of branching generations which is reflected in the distribution of acinar path lengths as shown in Fig. 14; the mean is 8.25 mm with a standard deviation of ±1.41 mm. Fig. 16 shows the distribution of path length from the larynx to conducting airways of 2 mm diameter, as estimated on a

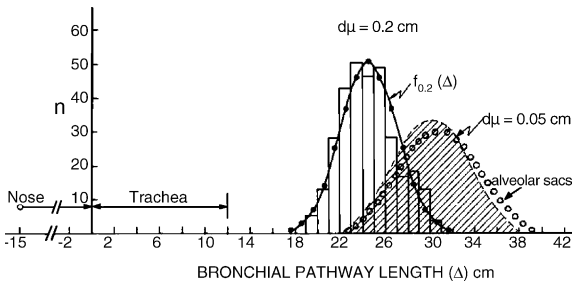

Fig. 16. Distribution of total airway path length in human lung. On the basis of the measurement of path length distribution of conducting airways (histogram, Weibel, 1963) the distribution of airways with a diameter of 0.5 mm is estimated (hatched curve). This corresponds approximately to the path length from the trachea out to the transitional bronchioles, the entrance to the acini. From Fig. 14, we can estimate that the acinar airways add 6–12 mm to this path length yielding a distribution curve as shown with open circles. From Sapoval et al. (2002).

bronchial tree cast (Weibel, 1963), and the extrapolation to 0.5 mm bronchioles which would correspond to the transitional bronchioles leading into the acinus. The path length distribution of intra-acinar airways (Fig. 14) can be convoluted with this distribution to estimate the distribution of total path lengths of airways, from the origin to the terminal alveolar sacs. It is seen that the acinar path length (range 0.6–1.2 cm, mean 0.83 cm) adds very little to the total path length and its distribution over a range of 22–40 cm.

6. Implications of acinar design for gas exchange function: the phenomenon of diffusion screening in acinar airways

The gas exchange in the pulmonary acinus involves several physico-chemical phenomena that occur within the complex acinar geometry described above. For instance, in the distal regions of the lung, oxygen is transported towards the alveolar membrane both by convection and by molecular diffusion. Oxygen then diffuses through the tissue membrane into the blood, where it is bound by hemoglobin. Several physical parameters govern oxygen uptake at the acinar level, such as air velocity, the diffusion coefficient of oxygen in air, the alveolar membrane permeability, the blood hemoglobin content and its reaction rate with oxygen. Conversely, carbon dioxide is discharged from the blood to the alveolar gas through diffusion across the membrane. It then diffuses backwards along the airways to the zone where convection becomes dominant, and is lastly expelled from the lung. In all these processes, the morphology of the system plays an essential role.

Lacking direct measurements of the distribution of oxygen (or carbon dioxide) concentration in the acinus, several mathematical models have been developed and studied by numerical simulations. In an early model, incomplete intrapulmonary gas mixing, called stratification, was assigned to the finite diffusivity of oxygen, preventing it to spread evenly in the acinus within an inspiration period (Scheid and Piiper, 1980).

Later on, the respective roles of convection and diffusion in the gas mixing process were examined through numerical simulations (Paiva and Engel, 1985, 1987; Dutrieue et al., 2000; Tawhai and Hunter, 2001). These studies showed that concentration gradients may exist as a consequence of efficient capture of oxygen by hemoglobin, the permeability of the alveolar membrane being considered as infinite.

More recently, it has been shown that the finite permeability of the membrane plays a dominant role in the effective properties of the acinus as the gas exchange unit (Sapoval et al., 2002). In particular, this parameter determines the occurrence of concentration gradients due to a phenomenon known as *diffusional screening*, a classical phenomenon which occurs in systems that obey the Laplace equation, the stationary form of the diffusion equation which describes in 3D the conservation of particles obeying Fick's law:

Diffusional screening (sometimes referred to as diffusional limitation) means that O_2 molecules entering the diffusion unit (the subacinus) have a larger probability to hit the surface of the alveolar membrane near the entrance than in the more distal regions. If the membrane permeability is large, O_2 molecules are absorbed at the very first hits. As a consequence, part of the surface, corresponding to the deeper regions, is not active for absorption (Sapoval et al., 2002; Felici et al., 2003, 2004). These regions would then be of no use; they are *screened*. In contrast, if the permeability is small, molecules will be absorbed only after many collisions with the wall. They then have a fair chance to reach the deeper regions and the entire acinar surface will be effective for gas exchange. The existence of concentration gradients in the acinus, due to the serial arrangement of alveoli along the pathways, was suggested by Weibel (1984) and the fact that diffusional screening was a quantitative criterion for acinar morphology in mammals was indicated by Sapoval (1994).

More complete studies (Sapoval et al., 2002; Felici et al., 2003, 2004, 2005; Grebenkov et al., 2005) have shown in great detail that the role of screening is determined by the relative value of a physical length called Λ as compared to a morphological length L_p, the mean perimeter of a planar cut of the acinus. The physical length Λ_X for a gas species X is the ratio between its diffusivity D_X in the gas phase and its permeability W_X through the surface (air–blood barrier). It is therefore different for O_2 and CO_2 and also different in heliox or other gas mixtures. In the following, we recall the essential hypothesis and results of these studies.

7. What is the "diffusion cell" in the human acinus and how is it modified by exercise?

As discussed above, the occurrence of partial pressure gradients depends on both the gas diffusivity and permeability but also on the size of the diffusion cell. By "diffusion cell", we mean here the part of the acinus where convection can be reasonably neglected. The transition between convection and diffusion is described by the value of the "acinus Peclet number" P_a which compares the air drift velocity U with the mean diffusion velocity to reach the deeper regions of the acinus. At any branching generation Z, the distance to cross to the end of the sacs is of order $(Z_{max} - Z)\lambda$ where λ is the mean length of an acinar duct (Fig. 13, Table 2). Following (Sapoval et al., 2002) we define the "acinus Peclet number" P_a as

$$P_a = \frac{U(Z)(Z_{max} - Z)\lambda}{D_{O_2,air}} \quad (5)$$

where the flow velocity $U(Z)$ at stage Z is found from the branched airway morphometry, in particular the progressive increase of total cross-section (Table 2). Note that this number is different from the classical Peclet number, which is the velocity times the ratio between diameters over diffusion coefficient. The velocity $U(Z)$ depends on the breathing regime. For humans under exercise conditions, the air velocity is increased by a factor of order 10 above rest at all levels of the airway tree due to increased tidal volume and respiratory frequency (Weibel, 1984; Sapoval et al., 2001). The resulting values of P_a are shown in Fig. 17 for the human lung.

One can note the logarithmic scale of the ordinate in the figure. It indicates that the Peclet number, and thus the convection velocity, varies very rapidly from one generation to the next (due to the dichotomous structure of the bronchial tree). Consequently, the size of the part of the acinus considered as working in a purely diffusive manner remains approximately constant, whether inspiration or expiration is considered.

One also observes that the convection–diffusion transition ($P_a = 1$) occurs for $(Z_{max} - Z)$ of order 5 at rest and 2 in exercise. As a consequence, the diffusion cell at rest is approximately a 1/8 subacinus while at exercise it is a (much smaller) 1/64 subacinus.

Using an average $(Z_{max} - Z)$ value of order 2, one can estimate that, in the human lung, the part of the

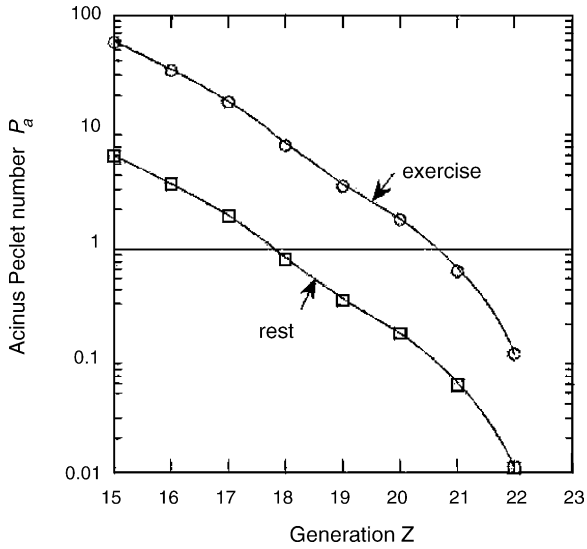

Fig. 17. Variation of the human acinus Peclet number at exercise and at rest as a function of the depth in the acinar pathway. One observes a large shift between rest and exercise. The transition from convection to diffusion is moved from generation 18 to 21. From Sapoval et al. (2002).

exchanger where O_2 is moved purely by diffusion has a volume of the order of $V_a/16 \approx 1.4 \times 10^{-3}\,cm^3$. The corresponding surface is also divided by 16 while the diameter L_p is divided by 2.5. The perimeter L_p of such a subregion of the acinus is then of the order 2.3 cm, now much smaller than the length $\Lambda_{O_2} \sim$ 30 cm (Table 3). This suggests that, under exercise conditions, the region beyond $Z = 21$ may behave as an optimized (i.e. unscreened) diffusion cell. This may appear as a small part of the lung, but it must be remembered that the last two generations of acinar airways contain 75% of the gas exchange surface.

In order to accurately estimate the influence of diffusional screening, the cyclic character of the breathing regime also should be considered. The above analysis relates only to the inspiration phase of the respiratory cycle when the diffusion source is gradually moved into the acinus. During expiration, however, the conditions are completely different. The convection–diffusion transition point moves towards the bronchi so that strong diffusion screening should exist during expiration. This effect should be particularly strong in exercise because the gas velocity is multiplied by a factor of 10 as compared to rest. The

Table 3
Parameters and computed quantities for different gas mixtures in a Kitaoka model acinus (Kitaoka et al., 2000)

	D_X ($cm^2\ s^{-1}$) (data)[a]	W_X ($cm\ s^{-1}$) (data)[b]	Λ_X (cm) (data)	$\eta(\Lambda_X)$ (simulation)	$W_X\ \eta(\Lambda_X)$ ($cm\ s^{-1}$) (simulation)
O_2 in air	0.19	0.79×10^{-2}	25	0.33	0.26×10^{-2}
CO_2 in air	0.17	0.16	1.0	0.04	0.64×10^{-2}
O_2 in heliox	0.73	0.79×10^{-2}	92	0.60	0.47×10^{-2}
CO_2 in heliox	0.61	0.16	3.8	0.09	1.12×10^{-2}
CO_2 in O_2	0.15	0.16	0.94	0.03	0.48×10^{-2}

[a] From Reid et al. (1987).
[b] From Weibel et al. (1993).

peak oxygen flux in exercise then corresponds to an unscreened regime only during a fraction of the respiratory cycle, namely when the diffusion source is deep inside the sub-acinus, i.e. during or at the end of inspiration. In other terms, the effective duty cycle of the system could have a value significantly smaller than 1.

8. The results of the theory of screening in real acini

Once the diffusion cell is defined from the above discussion, one can try to predict the role of diffusional screening in a quantitative manner. This has been done recently in several steps. We just recall here the results of the more realistic calculations (Felici et al., 2004, 2005) based on the *real* acinar topology described by Haefeli-Bleuer and Weibel (1988). The gas flux was computed in the eight real 1/8 sub-acini, represented in Fig. 10, under the hypothesis that blood can be considered as an oxygen sink at constant partial pressure (or a CO_2 source at constant partial pressure). The flux for a gas species X can be written as (Felici et al., 2005)

$$\Phi_X = kW_X\eta(\Lambda_X)P_X S_{alv} \tag{6}$$

where k is a constant, W_X the membrane permeability for X, $\eta(\Lambda_X)$ the subacinus efficiency, P_X the partial pressure difference between the subacinus entry and blood, and S_{alv} is the total alveolar surface of the lung. The subacinus efficiency $\eta(\Lambda_X)$ is a number smaller than 1, which represents the "equivalent" fraction of the surface, which is active for the exchange of the species X. The results of the computations of the efficiency for oxygen are shown in Fig. 18.

One observes that for oxygen at rest, the efficiency is found to be of order 33%. The same computations can be used to compute the flux for CO_2 and for various gas mixtures. The results are given in Table 3. In particular they permit to compute directly the oxygen partial pressure in venous blood by equating the O_2 and CO_2 flux expressed by the following equation:

$$\frac{P_{O_2}}{P_{CO_2}} = \frac{W_{CO_2}\eta(\Lambda_{CO_2})}{W_{O_2}\eta(\Lambda_{O_2})} = 2.5 \tag{7}$$

If we now suppose that the oxygen and CO_2 partial pressures at the acinus entry are respectively equal to

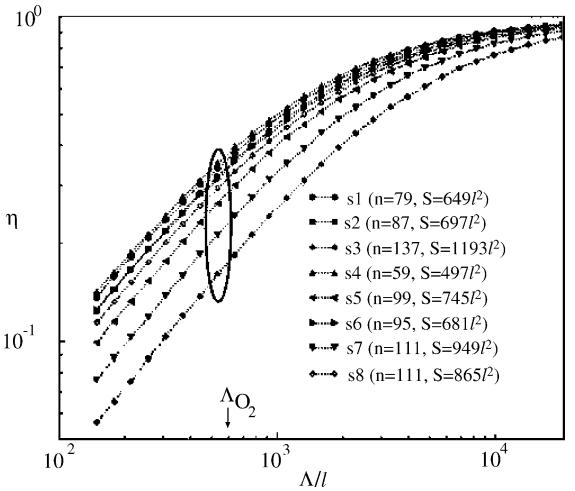

Fig. 18. Acinar efficiency η as a function of the physical length Λ for the eight subacini. Note that Λ is the ratio between diffusivity and permeability. Each curve represents the computed efficiency of each subacinus. For the parameter Λ corresponding to O_2 diffusion (noted on the horizontal axis), the efficiencies vary from 15 to 40% (inside ellipse), giving an average efficiency for the total acinus around 33%. From Felici et al. (2005).

150 and 0.3 mmHg and that the CO_2 partial pressure in blood is about 45 mmHg, one obtains (using the numbers in Table 3) that the oxygen partial pressure in venous blood is equal to 38.5 mmHg, a value very close to the measured value in the mixed venous blood 40 mmHg. It is a remarkable fact that, if one drops the concept of a uniform alveolar gas, the screening theory, applied to both oxygen and carbon dioxide, yields the known ratio of partial pressure differences. The numerical computations, discussed in (Felici et al., 2005), have been recently confirmed by an *analytical* study of the effect of screening in the acinus (Grebenkov et al., 2005).

9. What is the situation in exercise?

We have seen that in exercise, the convection–diffusion transition occurs in the region $(Z_{max} - Z)$ of order 2 (Fig. 17). The part of the exchanger where O_2 is moved purely by diffusion therefore has a volume of the order of $V_a/64 \approx 1.4 \times 10^{-3}$ cm^3 and the L_p of such a sub-region of the acinus is of order 2.3 cm, now much smaller than the length $\Lambda_{O2} \sim 25$ cm for oxygen (Table 3). This suggests that, under exercise conditions, the region beyond $Z = 21$ may behave as an optimized (i.e. unscreened) diffusion cell; Felici et al. (2005) estimated an efficiency of order 90%. In these conditions, the total lung diffusive conductance is $D_M = \beta D_{O_2,water} \times S_{alv}/\tau$ where S_{alv} is the total alveolar surface and τ barrier thickness. This can be computed from morphometric data (Eq. (3)) and compared to the experimental metabolic rates in exercise $\dot{V}_{O_2}$ max for humans (Table 1) and various mammals (Sapoval et al., 2002). One finds that, whatever the mass of a mammal, and whatever its aerobic capacity (athletic versus sedentary), its $\dot{V}_{O_2}$ max (a *purely physiological quantity*) is proportional to the *purely morphologic quantity* DM, as shown with great accuracy in Fig. 19.

However, this remarkable proportionality raises an important question (Sapoval et al., 2002). The value of the ratio $\dot{V}_{O_2}$ max/D_M implies that a partial pressure difference of the order of 10 Torr is sufficient to ensure O_2 uptake at $\dot{V}_{O_2}$ max. This appears too small by a factor of 3–5. To explain this seemingly too large value of D_M, three types of effects could be invoked: (1) the effective surface may be slightly overestimated but this cannot explain by itself such a factor. (2) In order to

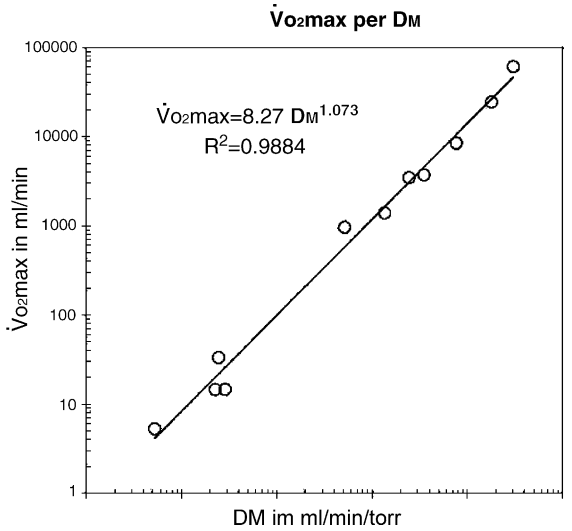

Fig. 19. Relation between the physiological value of maximal O_2 consumption, $\dot{V}_{O_2}$ max, and the morphometric value DM for various mammals (from left: woodmouse, white rat, guinea pig, mole rat, fox, goat, dog, pronghorn, human, steer, and horse). The exponent of the power law is 1.073.

achieve a high level of O_2 saturation of hemoglobin during the short transit time the P_{O_2} at the surface of erythrocytes must be positive, corresponding to about half the P_{O_2} at the alveolar surface, again not enough to explain this difference. (3) The theoretical estimation of the flux corresponding to $\dot{V}_{O_2}$ max should be revised. In particular one should question the assumption of steady state conditions to quantitatively explain gas exchange, especially in exercise. This ignores the fact that during the respiratory cycle there is a significant fraction of time during which the gas velocity is low particularly during expiration. During these low velocity periods two things happen. First, in a steady state that would correspond to these low velocities, the convection–diffusion transition is shifted towards the bronchi so that very strong screening should exist. Secondly, during the same periods, the time for diffusion becomes larger than the (accelerated) respiratory cycle. In other terms, there exists, in exercise, an effective duty cycle of the system which could have a value significantly smaller than 1. Note that both these phenomena are the consequence of finite diffusivity and screening, static versus dynamic conditions. The second of these phenomena is what was called stratification in the past. This discussion calls for a detailed study of

the convection–diffusion dynamics and its effects on screening.

10. Effects of the physical properties of gas mixtures on gas exchange

For physiological or therapeutic purposes, oxygen can be mixed with helium or other gases instead of nitrogen. This modifies both the viscosity of the mixture and the oxygen diffusivity. He–O_2 and SF_6–O_2 represent extremes in these terms, the viscosity increasing in the sequence He–O_2, air, SF_6–O_2 whereas the diffusivity decreases. Helium–oxygen is used in clinical situations where a physiological or a clinical benefit is anticipated from the reduction of the viscosity of the inhaled gas, in order to reduce the resistive work of breathing. This is, for example, the case in tracheal stenosis, acute severe asthma, or acute respiratory failure of chronic obstructive pulmonary disease (Schaeffer et al., 1999). In the latter two situations, the benefit may come not only from a reduced inspiratory resistive work of breathing, but also from a better emptying of pulmonary compartments with very slow time constants, leading to a lesser degree of dynamic hyperinflation and hence of elastic work of breathing. These changes interfere with diffusional screening. With helium–oxygen, the screening effect is expected the decrease, due to a larger Λ_X itself because of a higher oxygen diffusivity in helium. With SF_6–O_2 on the contrary, the screening effect is expected to increase, due to a lower Λ resulting from a lower oxygen diffusivity. Experimental data in the literature are compatible with these predictions and therefore lend support to the reality and relevance of acinar diffusional screening (Watson et al., 1987; Siddappa et al., 2003; Erickson et al., 1995). In most of the above studies, no particular explanation was proposed for the helium-related reduction in AaO_2. Erickson et al. (1995) attributed this observation to a “more complete diffusion equilibration”. All these results are compatible with acinar screening. However, it should be noted that Buono and Maly (1996) failed to observe any helium-related improvement in AaO_2 at maximal exercise in trained athletes even though the helium–nitrogen substitution resulted in an increased minute ventilation (up to 30 l/min). But, during exercise, the convection–diffusion transition occurs deeper in the acinus (Sapoval et al., 2002), so that efficiency is maximized and therefore becomes unresponsive to helium.

In the presence of helium-related acinar unscreening, the fall in AaO_2 automatically comes with an increased CO_2 clearance. Indeed, in the study by Siddappa (Siddappa et al., 2003), arterial P_{aCO_2} decreased as a function of helium concentration in the inhaled gas mixture, even though ventilation remains constant. This also is in accordance with the idea of de-screening due to helium.

Finally, it should be noted that the need for an adequate diffusion-perfusion matching (see above) is less important in the case of helium–oxygen than in the case of air, because of the lower oxygen partial pressure heterogeneity. This could be a useful feature in certain pathological situations where abnormalities of the structure and function of the pulmonary vasculature compromise hypoxic vasoconstriction. Conversely, under SF_6–O_2, diffusion-perfusion matching may be crucial for hemoglobin saturation.

11. Conclusions

This analysis has shown that the design properties of the peripheral airways, particularly their morphometric characteristics, are important determinants of the functional performance of the pulmonary gas exchanger. Optimization of gas exchange over a inner surface area the size of a tennis court demands that the O_2 supply and CO_2 discharge pathways are designed in such a way as to ensure that the entire surface, even its points most distant from the trachea, receive an adequate replenishment of O_2 for transfer to the blood. This is achieved by attaching the gas exchanging units as small acini at the end of a branched tree of conducting airways.

References

Bachofen, H., Weber, J., Wangensteen, D., Weibel, E.R., 1983. Morphometric estimates of diffusing capacity in lungs fixed under zone II and zone III conditions. Respir. Physiol. 52, 41–52.

Buono, M.J., Maly, R., 1996. Augmented hyperventilation via normoxic helium breathing does not prevent exercise-induced hypoxemia. Can. J. Appl. Physiol. 21, 264–270.

Cardoso, W.V., 2000. Lung morphogenesis revisited: old facts, current ideas. Dev. Dynamics 219, 121–130.

Dutrieue, B., Vanholsbeeck, F., Verbank, S., Paiva, M., 2000. A human acinar structure for simulation of realistic alveolar plateau slopes. J. Appl. Physiol. 89, 1859–1867.

Erickson, B.K., Seaman, J., Kubo, K., Hiraga, A., Kai, M., Yamaya, Y., Wagner, P.D., 1995. Hypoxic helium breathing does not reduce alveolar-arterial P_{O_2} difference in the horse. Respir. Physiol. 100, 253–260.

Felici, M., Filoche, M., Sapoval, B., 2003. Diffusional screening in the human pulmonary acinus. J. Appl. Physiol. 94, 2010–2016.

Felici, M., Sapoval, B., Filoche, M., 2004. Renormalized random walk study of oxygen absorption in the human lung. Phys. Rev. Lett. 92, 068101-1–068101-4.

Felici, M., Filoche, M., Straus, C., Similovski, T., Sapoval, B., 2005. Diffusional screening in real 3D human acini—a theoretical study. Respir. Physiol. Neuro. 145 (2–3), 279–293.

Gehr, P., Bachofen, M., Weibel, E.R., 1978. The normal human lung: ultrastructure and morphometric estimation of diffusion capacity. Respir. Physiol. 32, 121–140.

Gil, J., Bachofen, H., Gehr, P., Weibel, E.R., 1979. Alveolar volume-surface area relation in air- and saline-filled lungs fixed by vascular perfusion. J. Appl. Physiol. 47, 990–1001.

Grebenkov, D., Filoche, M., Sapoval, B., 2005. Diffusion-reaction in branched structures: theory and application to the lung. Phys. Rev. Lett. 94, 050602.

Haefeli-Bleuer, B., Weibel, E.R., 1988. Morphometry of the human pulmonary acinus. Anat. Rec. 220, 401–414.

Hess, W.R., 1914. Das Prinzip des kleinsten Kraftverbrauches im Dienste hämodynamischer Forschung Archiv für Anatomie und Physiologie. Physiologische Abteilung.

Horsfield, K., Dart, G., Olson, D.E., Filley, G.F., Cumming, G., 1971. Models of human bronchial tree. J. Appl. Physiol. 31, 207–217.

Horsfield, K., 1997. Pulmonary airways and blood vessels considered as confluent trees. In: Crystal, RG., West, JB., Weibel, ER., Barnes, PJ. (Eds.), The Lung: Scientific Foundations, vol. 1, second ed. Lippincott-Raven Publishers, Philadelphia, pp. 1073–1079.

Karas, R.H., Taylor, C.R., Jones, J.H., Lindstedt, S.L., Reeves, R.B., Weibel, E.R., 1987. Adaptive variation in the mammalian respiratory system in relation to energetic demand VII. Flow of oxygen across the pulmonary gas exchanger. Respir. Physiol. 69, 101–115.

Kitaoka, H., Tamura, S., Takaki, R., 2000. A three dimensional model of the human pulmonary acinus. J. Appl. Physiol. 88, 2260–2268.

König, M.F., Lucocq, J.M., Weibel, E.R., 1993. Demonstration of pulmonary vascular perfusion by electron and light microscopy. J. Appl. Physiol. 75, 1877–1883.

Mauroy, B., Filoche, M., Weibel, E.R., Sapoval, B., 2004. An optimal bronchial tree may be dangerous. Nature 427, 633–636.

Murray, C.D., 1926. The physiological principle of minimum work. I. The vascular system and the cost of blood. Proc. Natl. Acad. Sci. U.S.A 12, 207–214.

Paiva, M., Engel, L.A., 1985. Model analysis of intra-acinar gas exchange. Respir. Physiol. 62, 257–272.

Paiva, M., Engel, L.A., 1987. Theoretical studies of gas mixing and ventilation distribution in the lung. Physiol. Rev. 67, 750–796.

Reid, C., Prausnitz, J.M., Poling, B.E., 1987. The Properties of Gases and Liquids. McGraw-Hill, New York, San Francisco, Paris.

Rodriguez, M., Bur, S., Favre, A., Weibel, E.R., 1987. Pulmonary acinus: geometry and morphometry of the peripheral airway system in rat and rabbit. Am. J. Anat. 180, 143–155.

Sapoval, B., 1994. Transfer to and across irregular membranes modelled by fractal geometry. In: Nonnenmacher, T.F., Losa, G.A., Weibel, E.R. (Eds.), Fractals in Biology and Medicine. Birkhäuser-Verlag, Bâle, pp. 241–249.

Sapoval, B., Filoche, M., Weibel, E.R., 2001. In: Fleury, V., Gouyet, J.F., Leonetti, M. (Eds.), Branching in Nature. EDP Sciences, pp. 225–242.

Sapoval, B., Filoche, M., Weibel, E.R., 2002. Smaller is better but not too small, a physical scale for the mammalian pulmonary acinus. Proc. Natl. Acad. Sci. U.S.A. 99 (16), 10411–10416.

Schaeffer, E.M., Pohlman, A., Morgan, S., Hall, J.B., 1999. Oxygenation in status asthmaticus improves during ventilation with helium-oxygen. Crit. Care Med. 27, 2666–2670.

Scheid, P., Piiper, J., 1980. Intrapulmonary gas mixing and stratification. Pulm. Gas Exch. 1, 87–130.

Schreider, J.P., Raabe, O.G., 1981. Structure of the human respiratory acinus. Am. J. Anat. 162, 221–232.

Siddappa, R., Dowhy, M.S., Rotta, A.T., Hernan, L.J., Heard, C.M., Fuhrman, B.P., 2003. Heliox enhances carbon dioxide clearance from lungs of normal rabbits during low bias flow oscillation. Pediatr. Crit. Care Med. 4, 89–93.

Tawhai, M.H., Hunter, P.J., 2001. Characterizing respiratory airway gas mixing using a lumped parameter model of the pulmonary acinus. Respir. Physiol. 127, 241–248.

Watson, J., Kamm, R.D., Burwen, D.R., Brown, R., Ingenito, E., Slutsky, A.S., 1987. Gas exchange during constant flow ventilation with different gases. Am. Rev. Respir. Dis. 136, 420–425.

Weibel, E.R., Bachofen, H., 1987a. How to stabilize the pulmonary alveoli: surfactant or fibers? NIPS 2, 72–75.

Weibel, E.R., 1963. Morphometry of the Human Lung. Springer Verlag/Academic Press, Heidelberg, New York.

Weibel, E.R., 1984. The Pathway for Oxygen Structure and Function in the Mammalian Respiratory System. Harvard University Press, Cambridge.

Weibel, E.R., 1989. Lung morphometry and models in respiratory physiology. In: Chang, HK., Paiva, M. (Eds.), Respiratory Physiology: An Analytical Approach. Dekker, New York, pp. 1–56.

Weibel, E.R., 1997a. Design and morphometry of the pulmonary gas exchanger. In: Crystal, RG., West, JB., Weibel, ER., Barnes, PJ. (Eds.), The Lung: Scientific Foundations, vol. 1, second ed. Lippincott-Raven Publishers, Philadelphia, pp. 1147–1157.

Weibel, E.R., 1997b. Design of airways and blood vessels considered as branching trees. In: Crystal, RG., West, JB., Weibel, ER., Barnes, PJ. (Eds.), The Lung: Scientific Foundations, vol. 1, second ed. Lippincott-Raven Publishers, Philadelphia, pp. 1061–1071.

Weibel, E.R., Bachofen, H., 1987b. How to stabilize the pulmonary alveoli: surfactant or fibers? NIPS 2, 72–75.

Weibel, E.R., Bachofen, H., 1997. The fiber scaffold of lung parenchyma. In: Crystal, RG., West, JB., Weibel, ER., Barnes, PJ. (Eds.), The Lung: Scientific Foundations, vol. 1, second ed. Lippincott-Raven Publishers, Philadelphia, pp. 1139–1146.

Weibel, E.R., Federspiel, W.J., Fryder-Doffey, F., Hsia, C.C.W., König, M., Stalder-Navarro, V., Vock, R., 1993. Morphometric

model for pulmonary diffusing capacity I. Membrane diffusing capacity. Respir. Physiol. 93, 125–149.

Weibel, E.R., Gomez, D.M., 1962. Architecture of the human lung. Science 137, 577–585.

Weibel, E.R., Marques, L.B., Constantinopol, M., Doffey, F., Gehr, P., Taylor, C.R., 1987. Adaptive variation in the mammalian respiratory system in relation to energetic demand VI. The pulmonary gas exchanger. Respir. Physiol. 69, 81–100.

Weibel, E.R., Taylor, C.R., 1981. Design of the mammalian respiratory system. Respir. Physiol. 44, 1–164.

Weibel, E.R., Taylor, C.R., Hoppeler H, 1991. The concept of symmorphosis: a testable hypothesis of structure-function relationship. Proc. Natl. Acad. Sci. U.S.A. 88, 10357–10361.

Wilson, T.A., Bachofen, H., 1982. A model for mechanical structure of the alveolar duct. J. Appl. Physiol. 52, 1064–1070.